MDPI

Article

Compact 3 × 1 Matrix Converter Module Based on the SiC Devices with Easy Expandability

Patrik Resutík * and Slavomír Kaščák

Department of Mechatronics and Electronics, Faculty of Electrical Engineering and Information Technology, University of Zilina, 010 26 Žilina, Slovakia; slavomir.kascak@feit.uniza.sk
* Correspondence: patrik.resutik@feit.uniza.sk

Abstract: This paper discusses a new approach for building a compact all-in-one matrix converter module based on SiC semiconductors arranged in a common source connection. The used transistors are in the D2PAK package. The design of the module is divided into two parts, namely a power module designed at one-layer aluminum substrate printed circuit board (PCB) to ensure good thermal performance and voltage isolation between the module and heatsink. The second board is responsible for the SiC driving and is mounted at the top of the power PCB and consists of metal-oxide semiconductor field effect transistor (MOSFET) drivers, isolated power supplies, a current direction detection circuit, and current value sensors. In the paper, the proper function of the SiC MOSFET drivers, current direction detection, and current measurement sensors were evaluated. Finally, 3D design together with the final prototype is presented. The modules contain three bidirectional cells for interconnection three input voltage sources and one output phase. The uniqueness and novelty of the presented module are the compactness and easy expandability of the module to achieve higher power outputs and multiphase applications such as five phase machines.

Keywords: matrix converter; silicon carbide; matrix module; driver

Citation: Resutík, P.; Kaščák, S. Compact 3 × 1 Matrix Converter Module Based on the SiC Devices with Easy Expandability. *Appl. Sci.* **2021**, *11*, 9366. https://doi.org/10.3390/app11209366

Academic Editors: Zbigniew Rymarski, Pooya Davari and Zbigniew Kaczmarczyk

Received: 3 September 2021
Accepted: 7 October 2021
Published: 9 October 2021

Publisher's Note: MDPI stays neutral with regard to jurisdictional claims in published maps and institutional affiliations.

Copyright: © 2021 by the authors. Licensee MDPI, Basel, Switzerland. This article is an open access article distributed under the terms and conditions of the Creative Commons Attribution (CC BY) license (https://creativecommons.org/licenses/by/4.0/).

1. Introduction

The popularity of the matrix converter increased in the last years [1,2] due to the possible advantages over the standard back-to-back converters (BBC). The improvement in the semiconductor industry, especially in the field of Silicon Carbide (SiC) and Gallium Nitride (GaN) transistors and the small footprint of the component, has opened new ways to build a compact and high-power density matrix converter. The main advantage of the matrix converter is the absence of the storage components (capacitor or inductor), which are getting bulkier if the output power of the standard BBC converter rises. The lack of storage components predetermines the matrix converter to applications with high-power density and it can be used in environments with low or high temperatures (for example, in aerospace applications). The market research shows that commercial products are not available nowadays for use in the matrix converter application. In the past, some power modules were designed and introduced. However, they are not available now due to the shortage of products, and researchers must design their module for the direct matrix converter (DMC) or indirect matrix converter (IMC). For the proper function of the converter, a bidirectional switch is required. The bidirectional switches are built from the discrete transistor in various configurations shown in Figure 1.

The first device is built from one semiconductor switch and four diodes, where the diode bridge is used. The advantage is that no complex commutation algorithm is required. The main disadvantage is the higher power losses, since the load current flows through three semiconductor devices [3]. The second configuration in Figure 1b, called the common emitter, is widely used due to its good dynamic parameters and lower power losses in comparison to the connection in Figure 1a [3]. The switch in Figure 1c is, from the loss point of view, the same as in Figure 1b but requires less isolated power supplies in the case

of a 3 × 3 converter [3,4]. The CC-switch configuration requires six power supplies, and the CE-switch configuration requires nine power supplies. The CC configuration has worse dynamic parameters due to the big collector parasitic inductance of the components [1]. The last structure is shown in Figure 1d and is represented by the RB-IGBT, which can block voltages in the reverse direction. However, their dynamic behavior in reverse recovery is very slow compared to the standard P-N diode, which can significantly raise the power losses. Because of the slow reverse recovery behavior, these types of switches are not much used in this application currently [5]. The experiments with the relatively new GaN technology show the potential of this technology to be used in future matrix converters applications [6–9].

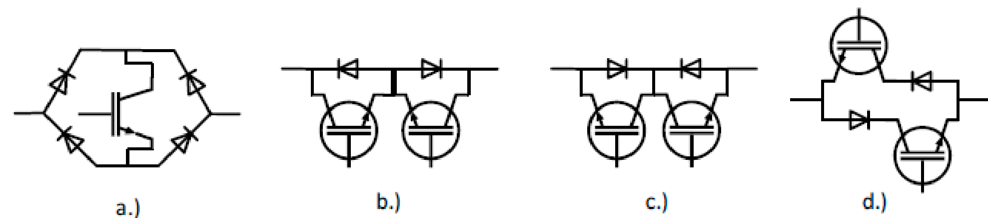

Figure 1. Possible types of the bidirectional switches: (**a**) diode bridge switch; (**b**) common-emitter (CE) switch; (**c**) common-collector (CC) switch; and (**d**) reverse blocking IGBT (RB-IGBT) switch.

These publications show the effort of the researchers to build a compact sample of the bidirectional switch for the matrix converter [10], where authors build an intelligent power switch module with implemented commutation in the module (since every module consists of a microcontroller in which the commutation algorithm is implemented). The next publications show a sample of the low parasitic inductance module based on the SiC chips from the CREE manufacturer [11,12]. The disadvantage of these modules is that if one device is destroyed, the whole module becomes useless, or the replacement of the broken component can be very expensive. A partial solution is presented in [13], where authors used D2PAK IGBTs mounted at the PCB in 3 × 1 configuration. This arrangement ensures good maintenance and reparability, but using the IGBT transistor leads to higher power losses which cannot be easily dissipated through FR4 substrate. So, additional cooling is required, especially at higher power outputs. Another approach presented by the authors in [14] offers a compact direct matrix converter using the SiC MOSFETs. The sample with a power of 2 kW was built in the PCB with dimensions of 358 × 155 × 40 mm. The high-density sparse matrix converter is presented in [15] with a very compact design wherein SiC MOSFETs were used. The power output of the converter is 1500 W, and the demonstrated power losses by the authors are below 80 W with a switching frequency of 100 kHz.

Several methods for cooling high-power surface mount technology (SMT) components are described in [16,17], as well as the impact of the vias placement on the cooling performance [18]. The first uses the thermal vias in the two-layer or multilayer PCB as shown in Figure 2a. The generated heat is dissipated through vias to the heatsink or the inner layers of the PCB. This method needs an additional insulating heat-conducting pad between the FR4 substrate and heatsink to ensure the right insulation of the board if high voltage is present. The next approach shown in Figure 2b, which can reach potentially lower thermal resistances, is PCB with copper inlays. This method is attractive from the low thermal resistance point of view but faces the same insulation problem. Additionally, non-standard manufacturing technology must be used, which can be costly, especially in small batches. The next solution on the market is the insulated metal substrate (IMS) boards, shown in Figure 2c, which ensure a good thermal interface between the SMT component and the heatsink with low thermal resistance provided by the metallic core. These PCBs are widely used in the automotive industry due to their good performance in the cooling of power LED modules. If electrical insulation is needed, manufacturers can offer IMS boards with an insulation voltage up to 4 kV. According to the datasheet of the used IMS board with the market name Goldenmax G11, the breakdown voltage is above 3 kV, declared by the manufacturer.

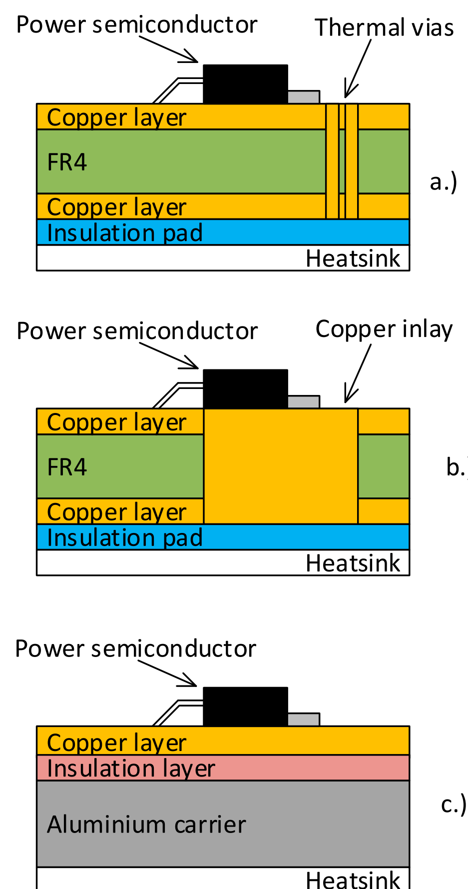

Figure 2. PCB Heat dissipation solution: (**a**) thermal vias; (**b**) copper inlay; (**c**) IMS board.

This paper focuses on the design, modeling, and practical realization of the 3 $\times$ 1 matrix converter module, with easy expandability to provide a matrix converter with various input/output configurations. According to the authors' research, no modules with similar parameters are now commercially available. The presented module can deliver power up to 1.7 kW. The designed module is part of the research project for the control of multiphase drives and the investigation of converter efficiencies. In the five-phase application, the presented modules in this configuration can deliver up to 8.5 kW. The output power of the module is adjustable by the change of power semiconductors and can be increased up to 3.5 kW per module.

2. Structure of the Module

The module was designed to be very compact, considering the mounting of almost all required components to drive the module, with only the need for external signals to control the module. Due to this consideration, the design was separated into three parts. The block diagram with the highlighted blocks is shown in Figure 3.

For the power part, the SiC transistors were used due to their relatively high operation temperature, high blocking voltage, and relatively small form factor. Recently, the ON-Semiconductors manufacturer released a new family of the SiC MOSFETs, which were well suited for this application. The semiconductors are in the D2PAK-7 package with a Kelvin source pin extended from the package to ensure proper driving of the device. It is important to select the right mounting of the semiconductors to ensure good electrical insulation and good heat dissipation. For this application, the best price to performance ratio is achieved by the IMS boards according to the research in the introduction. Additionally, this approach does not need an insulating pad between PCB and the heatsink, increasing thermal resistance significantly.

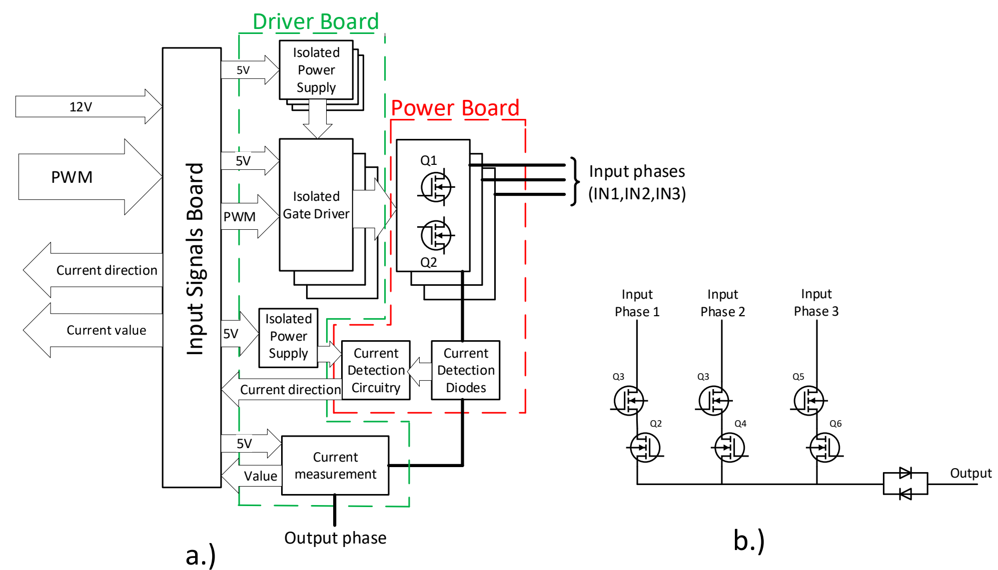

Figure 3. (**a**) Block diagram of the presented module, (**b**) schematic of the power part of the presented module.

For the power part, the common-source configuration of the switches was selected. As described in many publications [19–24], the commutation algorithm must be implemented to ensure no short or open circuit development, leading to overvoltage and overcurrent generation and circuit destruction. Many commutation techniques are available where most of them are based on the output current measurement. Thus, the authors decided to implement a current direction measurement to the power board for the commutation investigation in future work. The output current direction in the matrix converter can be measured in many ways, and these methods are summarized in Table 1, together with possible advantages and disadvantages.

Table 1. Comparison of the basic current direction measurement methods.

Method	Advantages	Disadvantages
Direct measurement at the transistors	-No additional losses -Accurate at low currents -No isolated power supply needed -Only one circuit per output phase	-Every transistor needs its circuitry -Lot of parts
Measuring at the output diodes	-Only one circuit per output phase -Accurate at low currents	-Enters additional losses to the converter -Needs an isolated power supply -Additional components
Measuring at the output shunt	-Only one circuit per output phase - Small additional losses	-Low accuracy at the small output currents -Needs an isolated power supply

Since the current direction detection circuitry is designed at the power IMS board, the authors selected a method that measures at the output diodes, offering good precision and fast reaction. The power losses can be effectively dissipated through the metal board to the heatsink. If the diodes with low drop voltage are selected, the power losses can be reduced significantly. The circuit is supplemented with the fast comparator to detect the voltage drop direction at the diodes, as shown in Figure 4. The board was designed to one-layer IMS board with final dimensions of 129 × 58 mm. The design of the power board is shown in Figure 4. The board consists of four mounting holes to be easily mounted to the heatsink.

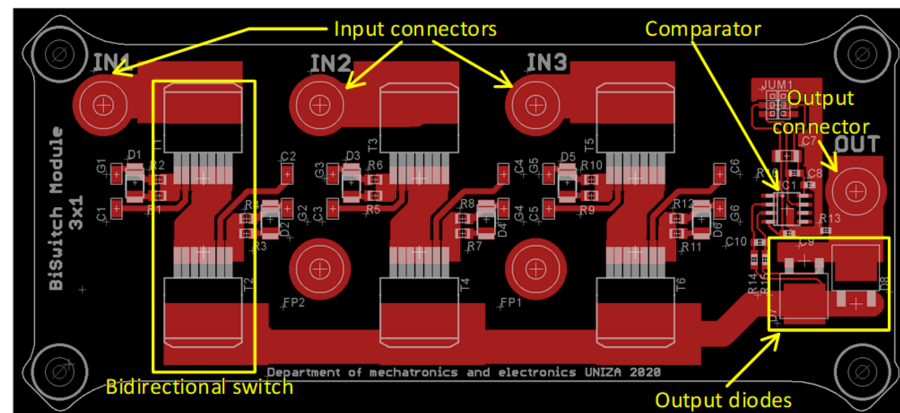

Figure 4. Design of the power IMS board.

The design of this board allows the change of the power devices based on the output power specification of the matrix converter. The 3D model of the power board is shown in Figure 5.

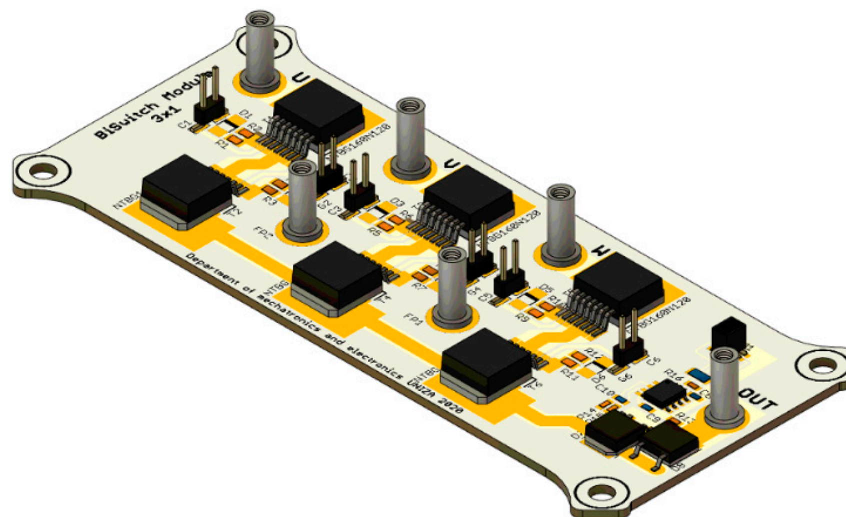

Figure 5. The 3D model of the power board.

The second board was designed for driving SiC transistors. The SiC transistors offering a high blocking voltage together with a low $R_{DS(on)}$ in comparison with traditional MOSFET technology. To ensure the short signal traces to the SiC MOSFET Gate pin, the driver board is placed right above the power board. The signals are transferred through the connectors. Since the input of the converter is connected to the phase voltage and a common source of transistors floats at the high voltage potentials, the isolated gate driver is needed. For the proper supply of the secondary side of the driver, the isolated push-pull power supply is designed based on the SN6505 push-pull driver to ensure a small form factor. The secondary voltage from the power supply is 18.5 V, and this voltage is further divided into +15.5 V and −3 V to ensure proper driving of the SiC power MOSFETs. For the gate driving, the dual isolated gate driver for the H-bridge applications was used. The secondary side of this driver was designed that way so that this driver can drive two transistors connected with a common source. The driver is capable of sourcing 4 A and sinking 6 A to each MOSFET. For proper SiC driving and ensuring that the driver is not overloaded by the current, the proper external gate resistors must be selected as shown in Figure 6. The following driving configuration was selected to ensure faster gate discharge and thus faster turn off times:

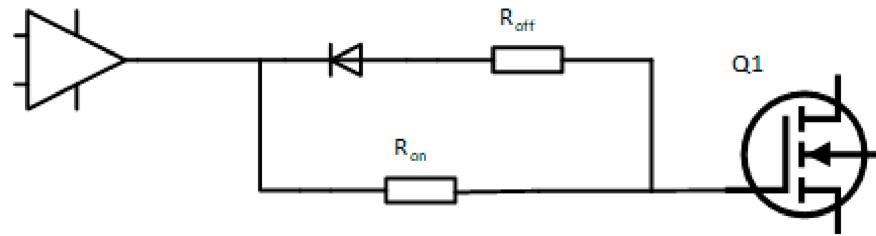

Figure 6. Configuration of the turn-on and turn-off resistors.

During the turn-on, only the R_{ON} resistor applies, since diode D is in the blocking direction. In the turn-off time, the diode is in the conducting stage and the resistors are connected in parallel, which allows reaching a higher discharge current. The resistors were selected as follows: R_{ON} = 4.1 Ω and R_{OFF} = 2.8 Ω. Then, the current capacity of the driver needs to be checked [25]:

$$I_{POS_MAX} = \frac{V_{DD} - V_{SS}}{\frac{R_{Nmos} \cdot R_{OH}}{R_{Nmos} + R_{OH}} + R_{ON} + R_{FETin}} \quad (1)$$

$$I_{NEG_MAX} = \frac{V_{DD} - V_{SS} - V_D}{R_{OL} + \frac{R_{ON} \cdot R_{OFF}}{R_{ON} + R_{OFF}} + R_{FETin}} \quad (2)$$

where R_{OH} and R_{OL} represent internal driver driving MOSFETs resistances, R_{Nmos} is internal pull-up driving resistor, and R_{ON}, R_{OFF}, and R_{FETin} represent the turn-on, turn-off, and SiC internal resistors, respectively, according to the SiC datasheet. Diode forward voltage is represented by V_D and supply voltages are denoted in V_{DD} for positive rail and V_{SS} for negative rail. The calculated values from (1) and (2) must be lower than 4 A for turn-on current (I_{POS_MAX}) and lower than 6 A for turn-off current (I_{NEG_MAX}) according to datasheet [25], to ensure that driver is not overloaded. In our case, the calculated results are 2.9 A and 5.2 A for I_{POS_MAX} and I_{NEG_MAX}, respectively. Calculated values are below the maximum values specified by the datasheet [25] which confirms the correctness of the design. All circuitry in the driver board is powered from the single 5 V power supply. The board includes a voltage supervisor IC, which ensures the power supplies startup when the supply voltage reaches 4.7 V by enabling the drivers to prevent current inrush.

Together with isolated power supplies and isolated gate drivers, the current measurement was implemented on this board. Current measurement is implemented on the driver board (Top PCB). The OUT pin shown in Figures 4 and 5 is used to conduct current from the power board to the driver board. Then, the current is flowing through the hall current sensor and then to the output phase pin shown in Figure 7. The sensor can measure current in the range of ± 20 A, which is suitable for this application, even if the SiC devices would be changed for more powerful ones. If the output current would be bigger, the manufacturer of the sensor offers a ± 30 A version in the same package, which can be easily changed if more output power is needed. Finally, the board involves a high-speed optocoupler, which ensures galvanic isolation and transfers the direction of the output current flowing through the module. The designed driver board is shown in Figure 7.

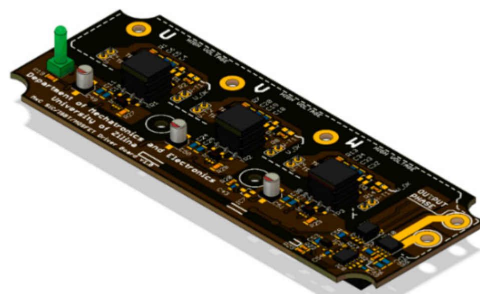

Figure 7. 3D model of the driver board.

The power and driver board are stackable with one another. The signal connections are made through pin headers. The connection of power high-voltage lines is made through steel-tinned standoffs. On the power board, the standoffs are soldered directly to the board, and in the driver board, the mounting screw is used. The assembled 3D model of the power and driver board is shown in Figure 8.

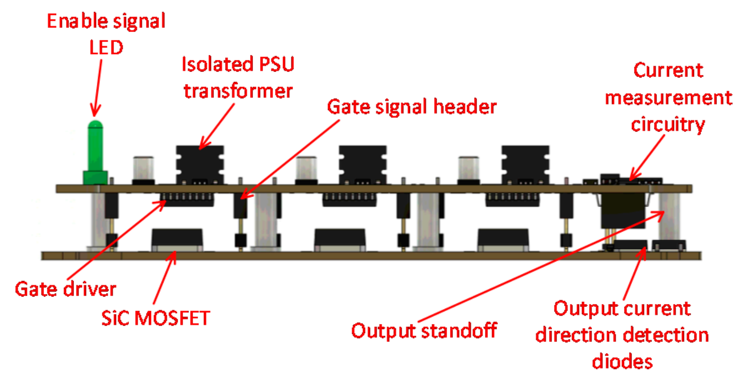

Figure 8. Cross-sectional look at the power and driver boards connection.

Due to the space limitations on the driver board, the input signal board shown in Figure 2 must be designed on the separated PCB. This board consists of a buck power supply with an operating range from 9 V to 15 V and output power of 10 W. For the interface, three different connectors are used. For the pulse width modulation (PWM) signals, the RJ50 shielded connector is used. This connector transfers six PWM signals, and the remaining wires are used as supply voltage lines. The level shifter shifts input PWM signals to the 5 V level appropriate for the gate drivers. For the current direction and the actual measured current value, the RJ11 connector is used. The value of the output module current is transferred through the differential twisted pair to improve immunity to electromagnetic interference. Finally, the optical TOS-LINK connector is added to the board. Through this interface, the current direction is transmitted too so that the board can transmit the current direction signal in two ways. The optical interface is fast, reliable, and immune to electromagnetic interference, so it is preferred in a disturbed environment. The signal board is mounted perpendicularly to the driver board, so all connectors face upwards. The 3D model of the assembled 3×1 matrix converter module is shown in Figure 9.

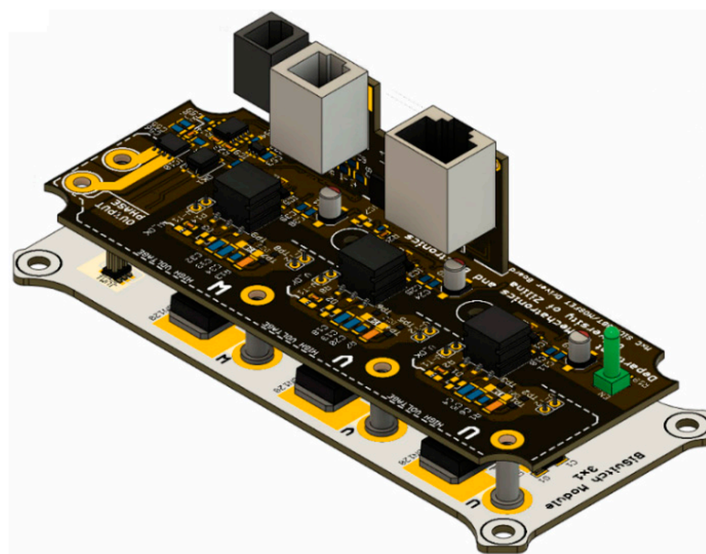

Figure 9. Assembled model of 3×1 matrix module.

For further protection against the accidental touch of the high voltage connectors, the cover was designed. The finalized module with the designed cover can be seen in Figure 10.

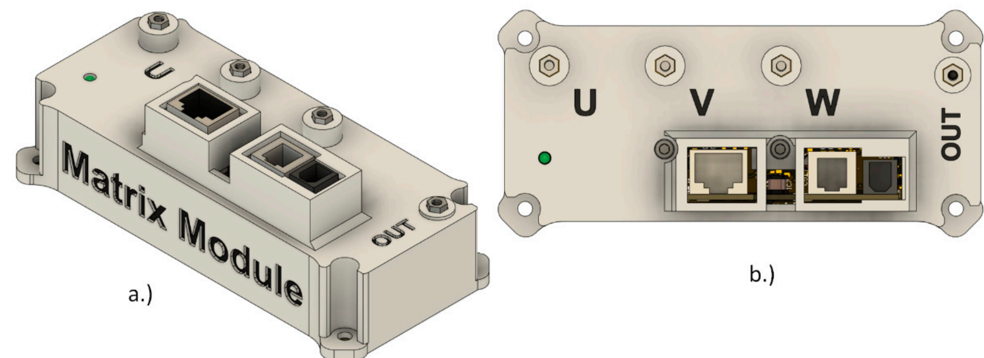

Figure 10. Assembled module: (**a**) Side view (**b**) Top view.

The final dimensions of one 3 × 1 matrix module are 130 × 54 × 43 mm (length × width × height). All PCBs were manufactured, and the final module was assembled according to designed 3D models.

3. Verification of the Operation

For the proper SiC MOSFETs driving, the isolated power supply must be capable of delivering at least 1 W of the power. The output power of the isolated power supply was measured together with an output voltage as a load current function. The efficiency was calculated from the measured data. The measured data of the power supply are shown in Figure 11.

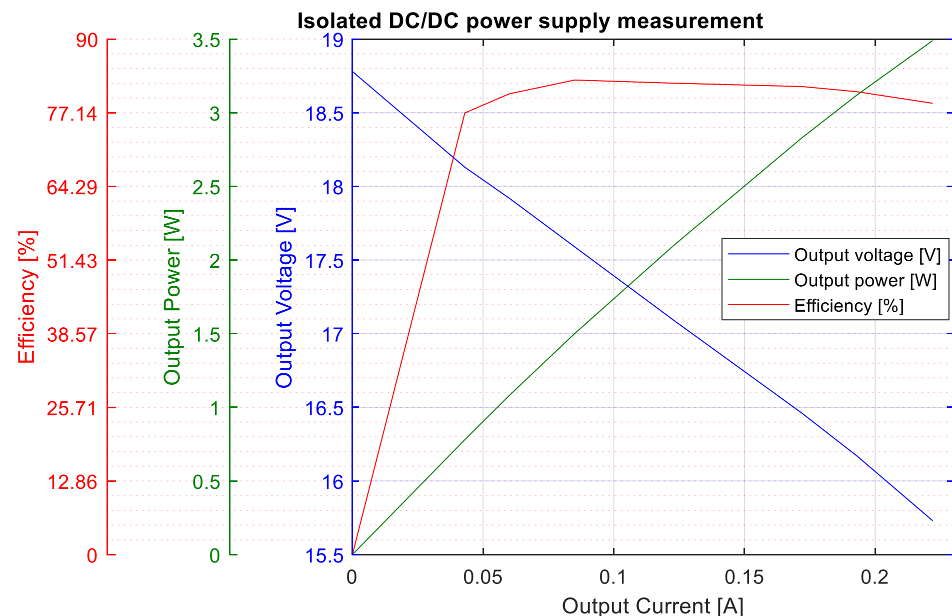

Figure 11. Measured characteristics of the designed isolated power supply.

As shown in Figure 11, the operating output power of approximately 1 W to 2 W converter reaches its maximum efficiency of around 82%. The converter can deliver more power in case if more powerful semiconductors are used. The output current is limited to 200 mA due to the used secondary rectification diode limitation. The thermal image of the one power supply during the output load of 2 W can be seen in Figure 12.

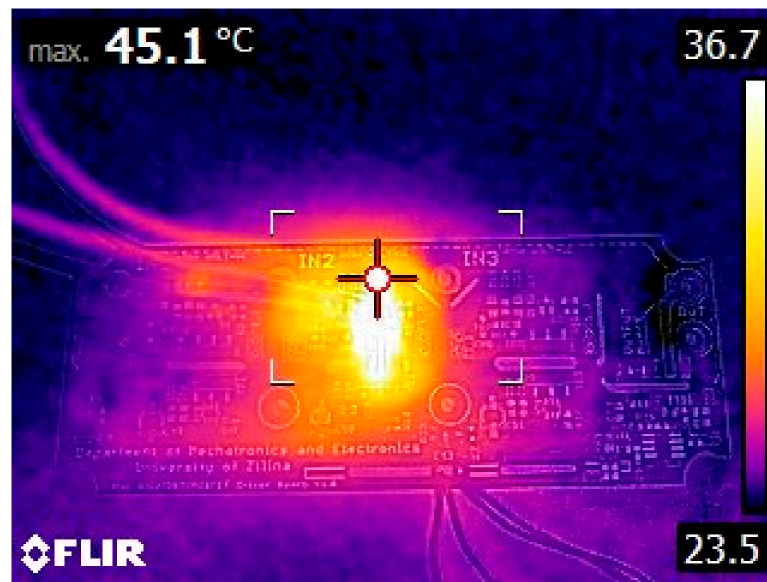

Figure 12. The temperature of the isolated power supply at the load of 2 W.

After the power supply efficiency and maximum load temperature, the most important indicator of the power supply quality is the output voltage waveform, especially during the startup of the power supply and dynamic events. If the overvoltage occurs during the startup, this can lead to the destruction of the semiconductor components. Thus, measuring the quality of the output waveform is important. The waveform of all of the voltages during the converter power supplies startup sequence can be seen in Figure 13.

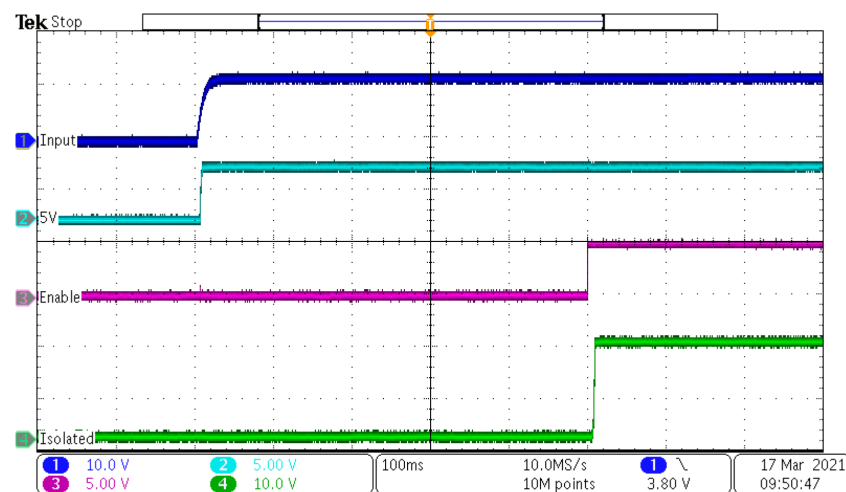

Figure 13. Power supply startup sequence (Input Voltage, Blue 10 V/div; 5 V Rail, Cyan 5 V/div; Enable Signal, Purple 5 V/div; Isolated Output, Green 10 V/div).

The Input signal represents the 12 V supply rail provided by the laboratory power supply. The 5 V rail is measured at the output of the buck converter. The Enable signal represents the signal from the supervisor circuit monitoring the 5 V rail. Finally, the Isolated signal is the voltage at the secondary side of the isolated power supply for the gate drivers. As shown in Figure 13, no overshoots are present, and the startup of the isolated power supply occurs after enabling signal when the 5 V supply rail is present and stable.

For the driver functionality verification, the PWM signal was applied to the input of the driver board, and the output signal was measured at the gate of the SiC MOSFET. The measured waveforms can be seen in Figure 14.

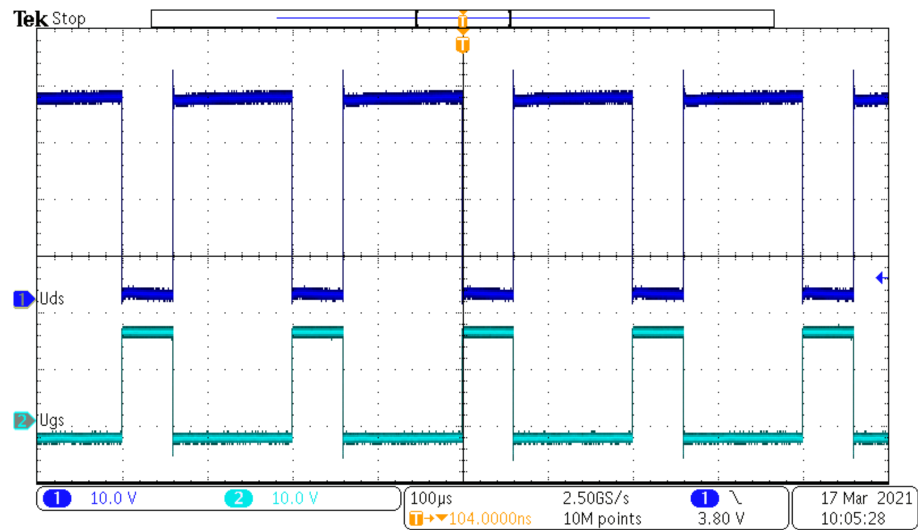

Figure 14. PWM signals (Blue, UDS voltage 10 V/div; Cyan, UGS voltage 10 V/div).

The cyan waveform in Figure 15 represents the output signal applied to the SiC MOSFET gate, where turn-off is represented by the −3 V and turn-on is represented by the +15 V, as was designed. In the isolated gate driver, the important parameter is the signal propagation delay from the non-isolated to the isolated side. The measured value of delay was 20 ns for the turn-on waveform and 25 ns for the turn-off waveform. These measured values correspond to the values in the driver datasheet.

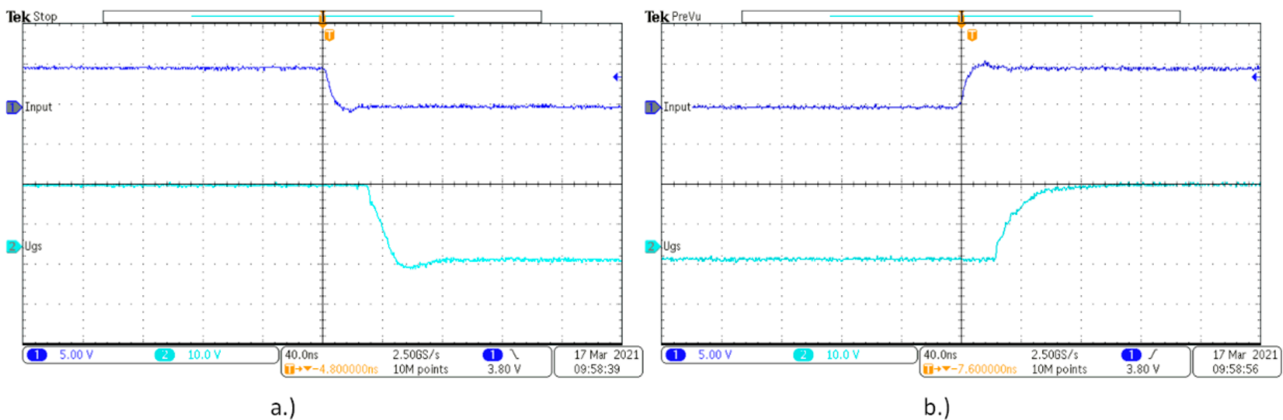

Figure 15. (**a**) turn-off delay; (**b**) turn-on delay; (Blue, Input waveform from generator 5 V/div; Cyan, UGS voltage 10 V/div).

One important aspect of the gate driver circuitry is the stability and the response of the isolated power supply. During the turn-on and turn-off process, the major current needs to be delivered or removed from the MOSFET gate. These currents are delivered mainly from the isolated power supply capacitors, and when the switching state is stable, the capacitors are recharged. If the voltage drop during the turn-on or turn-off transients is big, this can lead to a faulty transistor switch or can cause triggering under-voltage protection in the modern gate driver ICs. In this case, the single power supply needs to deliver the required power to the two transistors since the switch is bidirectional and constructed from two SiC devices connected by the common source. Measurement of the stability of the positive supply rail during turn-on and turn-off can be seen in Figure 16.

As can be seen in Figure 16, the power supply recovery from the turn-on transient last below 20 ns, with a negative overshoot of 1 V. For the turn-off process, the transient last below 50 ns with a positive overshoot of 1.9 V. At the end of turn-on or turn off process, the power supply rail is stable again.

In the next measurement, the output current detection circuit was measured. The isolated autotransformer was used to generate the AC waveform. The load for the AC waveform was a 33 Ω power resistor. The voltage oscilloscope probe measured the output of the current detector circuit, and the output current of the module was measured using a current probe (Tektronix TCP303). The current measurement designed at the board was evaluated too. The output of this sensor is the differential pair which represents the flowing current through a circuit. Differential output was selected due to its very high resistance to the surrounding interface. The measured results are shown in Figure 17.

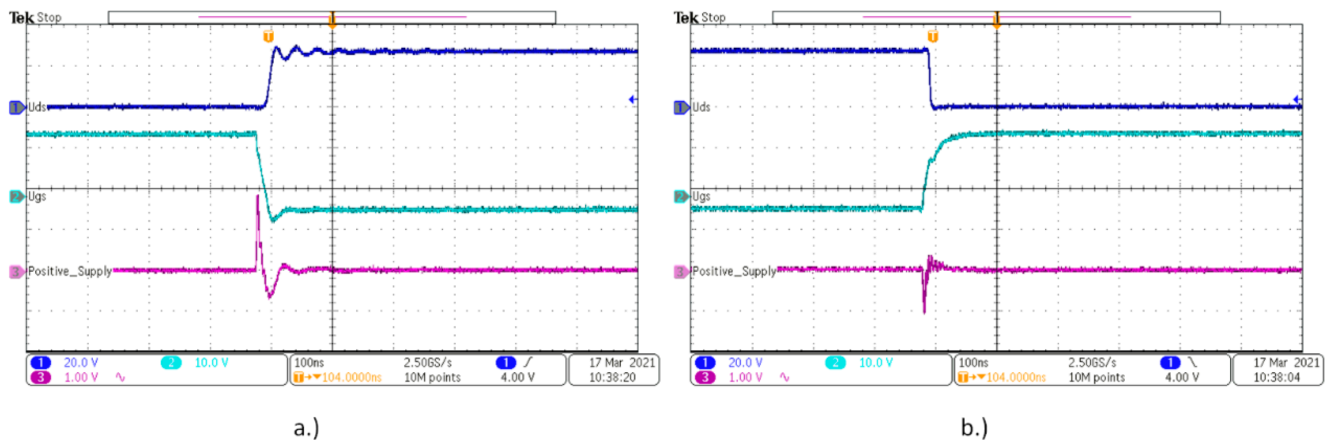

Figure 16. Power supply transients: (**a**) turn-off; (**b**) turn-on (Blue, UDS voltage 5 V/div; Cyan, UGS voltage 10 V/div; Purple, Isolated power supply positive rail 1 V/div; AC coupled).

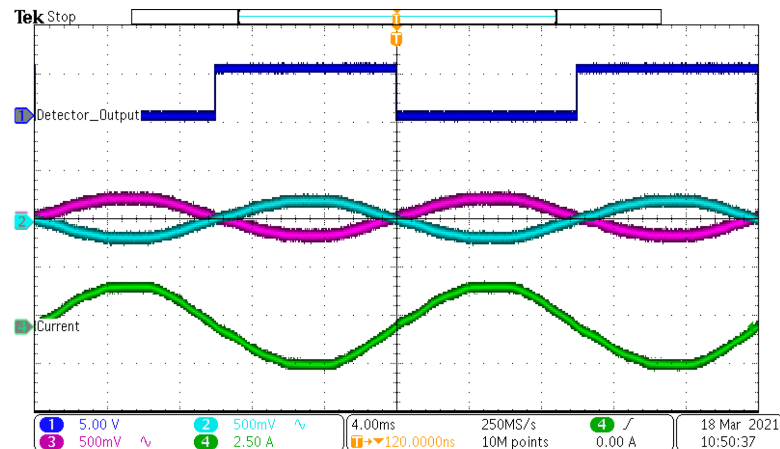

Figure 17. Current direction detection measurement (Blue, Current direction detector output 5 V/div; Green, Module current 2.5 A/div; Purple and Cyan, Differential outputs 500 mV/div).

As shown in Figure 17, the current detection circuit measures the direction of the output current reliably. The cyan and purple waveforms represent the differential outputs from the current value measurement circuitry. The signals are measured against the ground. For better visualization of the current detector functionality, the waveforms were measured with the same position settings, as shown in Figure 18.

The manufactured power board on the IMS with all power semiconductors assembled can be seen in Figure 19 at the left image. The top three spacers are used as connectors for input phases. The bottom two spacers are used as mounting and fixing supports for the higher rigidity of the module. The spacer mounted at the right side is the output phase connected to the driver board, where the current of this phase is measured. The assembled power board and the driver PCB can be seen in Figure 19 at the right side image.

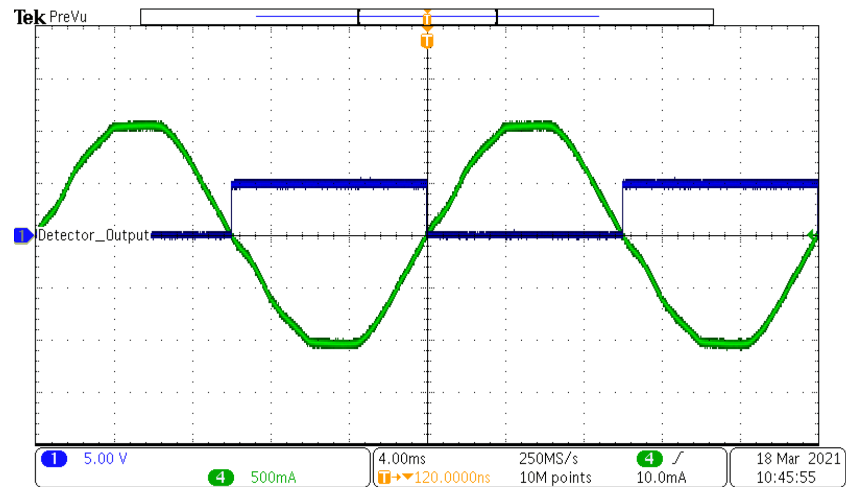

Figure 18. Current direction detection measurement (Blue, Current direction detector output 5 V/div; Green, Circuit current 500 mA/div).

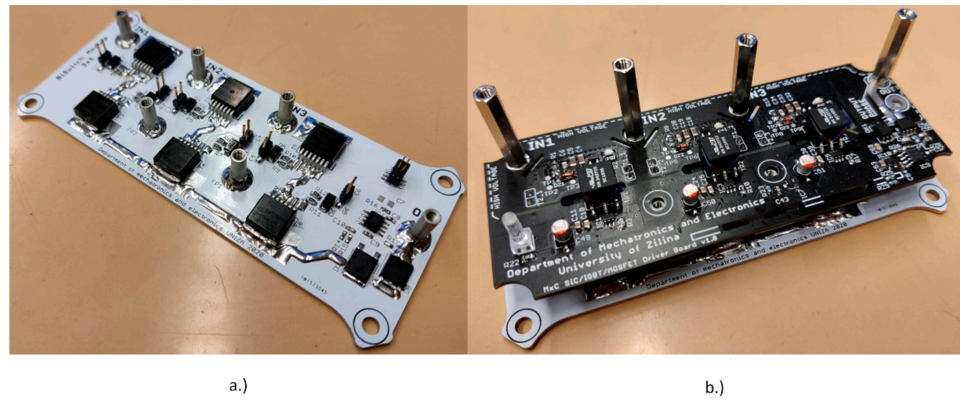

a.) b.)

Figure 19. (**a**) Power module on IMS boars (**b**) Assembled power module and driver board.

The designed cover for the compact matrix module presented in Figure 9 was tested too. The design was manufactured with the help of a 3D printer. The cover provides additional protection against accidental contact with the live parts of the module. The assembled module with the cover can be seen in Figure 20.

Figure 20. Assembled module with printed protection cover.

4. Discussion

The article aimed to present the design of the compact module suitable for use in matrix converter applications. The module is compact and allows different output powers with the dimensions of the module preserved. As mentioned in the introduction section, the power output of the module can be adjusted by the change of the power semiconductors in the IMS board. Due to easy expandability, the isolated power supply was designed with a sufficient power reserve to ensure that the higher power SiC will be driven properly. The output characteristics of the module can be seen in Figure 11. For the proper power-up sequence, the voltage supervisor circuitry is used with the voltage sequence measured in Figure 13. The driver capability of the dual-gate driver was measured too and can be seen in Figure 15. The propagation delay of the driver is within 30 ns as the manufacturer specified in the datasheet [25]. The response of the isolated power supply to the switching of the SiC was measured in Figure 16 for turn-on and turn-off transients. The functionality of the current direction detection circuitry, as well as current measurement circuitry, was tested and measured in Figures 17 and 18 respectively. Assembled module is shown in Figure 19, and the completed module together with 3D printed case is shown in Figure 20. The Table 2 summarizes used components in the presented module:

Table 2. Components used in the compact 3 × 1 matrix converter module.

Component	Marking
Power switch SiC	NTBG080N120SC1
Diode for current direction detection	V20PW15
SiC Driver	UCC21521
Current measurement sensor	ACHS-7192-500E
Input filter inductor	1 mH (external)
Input filter capacitor	7 µF/Delta connection (external)
Rated input voltage	3 × 230V RMS
Rated output power per module	1.7 kW

5. Conclusions

In this paper, the design of the compact, all-in-one matrix module is presented. The target of this design was implementing all needed circuitry to the one compact module. In this case, the module is in configuration 3 × 1. The easy expandability of these modules is another advantage; the module is ready to be interconnected to other modules via power bus bars, and therefore the various configurations of the resulting matrix converter can be easily constructed. The power part of the module is designed with SiC MOSFETs which offers high blocking voltage together with low conduction resistance, resulting in lower power losses in comparison with traditional MOSFET or IGBT structures. The power board prototype is designed on an IMS aluminum board containing power transistors in common-source configuration and current direction detection diodes. The main advantage of the usage of the IMS board is the maintenance of very good thermal dissipation from the power semiconductors to the heatsink along with high voltage insulation of the heatsink. On top of the IMS board the control board PCB is mounted which includes power drivers for every bidirectional switch together with isolated power supplies and current measurement sensor. The isolated power supply reaches 82% peak efficiency and has a maximum output power of 3.5 W. The assembled module uses two connectors. The first connector (RJ50) is used to transfer PWM signals and supply voltage to the module. The second connector (RJ11) is transferring current detection and current measurement signal to the supervisory control board for control and commutation purposes.

For the proper module functionality, the supervisory control board with a control algorithm generating all PWM signals for the used matrix converter modules is needed. This board will be included in future work and evaluation of the power board and construction of the matrix converter in configuration 3×5 with the use of the presented all-in-one modules.

Author Contributions: Conceptualization, P.R. and S.K.; methodology, P.R.; validation, S.K. and P.R.; formal analysis, P.R.; investigation, P.R. and S.K.; resources, P.R. and S.K.; writing—original draft preparation, P.R.; writing—review and editing, S.K.; visualization, P.R.; supervision, S.K.; project administration, S.K.; funding acquisition, S.K. All authors have read and agreed to the published version of the manuscript.

Funding: This research was funded by VEGA 1/0085/21, "Research of methods for increasing the efficiency of electric multiphase motor drive systems for automotive applications".

Institutional Review Board Statement: Not applicable.

Informed Consent Statement: Not applicable.

Conflicts of Interest: The authors declare no conflict of interest.

References

1. Bento, A.; Paraíso, G.; Costa, P.; Zhang, L.; Geury, T.; Pinto, S.F.; Silva, J.F. On the Potential Contributions of Matrix Converters for the Future Grid Operation, Sustainable Transportation and Electrical Drives Innovation. *Appl. Sci.* **2021**, *11*, 4597. [CrossRef]
2. Wang, R.; Huang, M.; Lu, C.; Wang, W. A Direct Three-Phase AC–AC Matrix Converter-Based Wireless Power Transfer System for Electric Vehicles. *Appl. Sci.* **2020**, *10*, 2217. [CrossRef]
3. Wheeler, P.W.; Rodriguez, J.; Clare, J.C.; Empringham, L.; Weinstein, A. Matrix converters: A technology review. *IEEE Trans. Ind. Electron.* **2002**, *49*, 276–288. [CrossRef]
4. Empringham, L.; Kolar, J.W.; Rodriguez, J.; Wheeler, P.W.; Clare, J.C. Technological Issues and Industrial Application of Matrix Converters: A Review. *IEEE Trans. Ind. Electron.* **2013**, *60*, 4260–4271. [CrossRef]
5. Grbovic, P.J.; Gruson, F.; Idir, N.; le Moigne, P. Turn-on Performance of Reverse Blocking IGBT (RB IGBT) and Optimization Using Advanced Gate Driver. *IEEE Trans. Power Electron.* **2010**, *25*, 970–980. [CrossRef]
6. Hirota, T.; Inomata, K.; Yoshimi, D.; Higuchi, M. Nine Switches Matrix Converter Using Bi-directional GaN Device. In Proceedings of the 2018 International Power Electronics Conference (IPEC-Niigata 2018—ECCE Asia), Niigata, Japan, 20–24 May 2018; pp. 3952–3957. [CrossRef]
7. Guerriero, P.; Orcioni, S.; Matacena, I.; Daliento, S. A GaN based bidirectional switch for matrix converter applications. In Proceedings of the 2020 International Symposium on Power Electronics, Electrical Drives, Automation and Motion (SPEEDAM), Sorrento, Italy, 24–26 June 2020; pp. 375–380. [CrossRef]
8. Nagai, S.; Yamada, Y.; Negoro, N.; Handa, H.; Kudoh, Y.; Ueno, H.; Ishida, M.; Otuska, N.; Ueda, D. 30.5 A GaN 3×3 matrix converter chipset with Drive-by-Microwave technologies. In Proceedings of the 2014 IEEE International Solid-State Circuits Conference Digest of Technical Papers (ISSCC), San Francisco, CA, USA, 9–13 February 2014; pp. 494–495. [CrossRef]
9. Umeda, H.; Yamada, Y.; Asanuma, K.; Kusama, F.; Kinoshita, Y.; Ueno, H.; Ishida, H.; Hatsuda, T.; Ueda, T. High power 3-phase to 3-phase matrix converter using dual-gate GaN bidirectional switches. In Proceedings of the 2018 IEEE Applied Power Electronics Conference and Exposition (APEC), San Antonio, TX, USA, 4–8 March 2018; pp. 894–897. [CrossRef]
10. Galvez, J.L.; Jorda, X.; Vellvehi, M.; Millan, J.; Jose-Prieto, M.A.; Martin, J. Intelligent bidirectional power switch module for matrix converter applications. In Proceedings of the 2007 European Conference on Power Electronics and Applications, Aalborg, Denmark, 2–5 September 2007; pp. 1–9. [CrossRef]
11. Hayes, J.K.; Escobar-Mejía, A.; Balda, J.C.; Dutta, A.; Ang, S.S. Realization of a SiC module-based indirect matrix converter with minimum parasitic inductances. In Proceedings of the 2014 IEEE Applied Power Electronics Conference and Exposition—APEC 2014, Fort Worth, TX, USA, 16–20 March 2014; pp. 587–594. [CrossRef]
12. Escobar-Mejia, A.; Stewart, C.; Hayes, J.K.; Ang, S.S.; Balda, J.C.; Talakokkula, S. Realization of a Modular Indirect Matrix Converter System Using Normally Off SiC JFETs. *IEEE Trans. Power Electron.* **2014**, *29*, 2574–2583. [CrossRef]
13. Gutiérrez-Torres, D.A.d.J.; Lozano-García, J.M.; Merchan-Villalba, L.R.; Pizano-Martínez, A.; Martínez-Patiño, J. Low Cost Practical Implementation of a Three-Phase Matrix Converter. In Proceedings of the 2019 IEEE International Autumn Meeting on Power, Electronics and Computing (ROPEC), Ixtapa, Mexico, 13–15 November 2019; pp. 1–7. [CrossRef]
14. Koiwa, K.; Itoh, J. Evaluation of a maximum power density design method for matrix converter using SiC-MOSFET. In Proceedings of the 2014 IEEE Energy Conversion Congress and Exposition (ECCE), Pittsburgh, PA, USA, 14–18 September 2014; pp. 563–570. [CrossRef]
15. Friedli, T.; Round, S.D.; Kolar, J.W. A 100 kHz SiC Sparse Matrix Converter. In Proceedings of the 2007 IEEE Power Electronics Specialists Conference, Orlando, FL, USA, 17–21 June 2007; pp. 2148–2154. [CrossRef]
16. Šír, M.; Feňo, I. Cooling of minimized sourface-mount packages in power electronics applications. *Prz. Elektrotechn. Vol.* **2020**, *11*, 151–154.
17. Fan, A.; Bonner, R.; Sharratt, S.; Ju, Y.S. An innovative passive cooling method for high performance light-emitting diodes. In Proceedings of the 2012 28th Annual IEEE Semiconductor Thermal Measurement and Management Symposium (SEMI-THERM), San Jose, CA, USA, 18–22 March 2012; pp. 319–324. [CrossRef]

18. Shen, Y.; Wang, H.; Blaabjerg, F.; Zhao, H.; Long, T. Thermal Modeling and Design Optimization of PCB Vias and Pads. *IEEE Trans. Power Electron.* **2020**, *35*, 882–900. [CrossRef]
19. Empringham, L.; Wheeler, P.; Clare, J. Power density improvement and robust commutation for a 100 kW Si-SiC matrix converter. In Proceedings of the 2009 13th European Conference on Power Electronics and Applications, Barcelona, Spain, 8–10 September 2009; pp. 1–8.
20. Haruna, J.; Miura, K.; Funato, H. A Consideration of 3-Step Commutation Method for Voltage Source Three-Phase/Single-Phase Matrix Converter. In Proceedings of the 2018 21st International Conference on Electrical Machines and Systems (ICEMS), Jeju, Korea, 7–10 October 2018; pp. 2301–2305. [CrossRef]
21. Ma, X.; Dong, H.; Zhao, J. Research on a novel two-step commutation strategy for matrix converter based on the value of input voltage. In Proceedings of the 2016 Chinese Control and Decision Conference (CCDC), Yinchuan, China, 28–30 May 2016; pp. 6988–6993. [CrossRef]
22. Herrero, L.C.; de Pablo, S.; Martin, F.; Ruiz, J.M.; Gonzalez, J.M.; Rey, A.B. Comparative Analysis of the Techniques of Current Commutation in Matrix Converters. In Proceedings of the 2007 IEEE International Symposium on Industrial Electronics, Vigo, Spain, 4–7 June 2007; pp. 521–526. [CrossRef]
23. Wang, X.; Lin, H.; She, H.; He, B. Implementation of two-step voltage commutation matrix converter. In Proceedings of the 2009 IEEE 6th International Power Electronics and Motion Control Conference, Wuhan, China, 17–20 May 2009; pp. 1728–1733. [CrossRef]
24. Ziegler, M.; Hofmann, W. Semi natural two steps commutation strategy for matrix converters. In Proceedings of the PESC 98 Record. 29th Annual IEEE Power Electronics Specialists Conference (Cat. No.98CH36196), Fukuoka, Japan, 22 May 1998; Volume 1, pp. 727–731. [CrossRef]
25. UCC21521 Datasheet. Available online: https://www.ti.com/lit/ds/symlink/ucc21521.pdf?ts=1632979759623&ref_url=https%253A%252F%252Fwww.ti.com%252Fproduct%252FUCC21521 (accessed on 20 August 2021).